Evidence for Discrete Triple-Network Coupling Architectures Orthogonal to Psychiatric Diagnosis

Alexander Campos
Independent Researcher
alex@guardian-labs.org

Abstract

We asked whether functional coupling among the Default Mode (DMN), Central Executive (CEN), and Salience (SN) networks clusters into discrete architectures in a transdiagnostic clinical sample. Resting-state fMRI data from 261 subjects were drawn from the UCLA Consortium for Neuropsychiatric Phenomics (OpenNeuro ds000030), all acquired on a single 3T Siemens scanner. fMRIPrep-preprocessed BOLD data were subjected to confound regression (6 motion parameters, 5 aCompCor components, framewise displacement, white matter signal); 11 subjects with mean FD > 0.5 mm were excluded, leaving $N = 249$ (118 controls, 48 bipolar, 45 schizophrenia, 38 ADHD). Gaussian mixture modeling of between-network coupling—applied both univariately (DMN-CEN) and multivariately (DMN-CEN, DMN-SN, CEN-SN)—strongly preferred a two-component solution in both cases (univariate: $\Delta\text{BIC} = 29.3$, bootstrap LR $p < 0.001$; multivariate: $\Delta\text{BIC} = 19.4$, bootstrap LR $p < 0.001$). Two coupling architectures emerged: a low-coupling cluster (75.9%) and a high-coupling cluster (24.1%). Diagnostic category did not predict cluster membership (ANOVA $p = 0.338$; χ^2 test $p = 0.748$). Coupling topology was orthogonal to psychiatric diagnosis in this sample.

Keywords: resting-state fMRI, default mode network, central executive network, salience network, triple-network model, functional coupling, mixture modeling, transdiagnostic

1 Introduction

Resting-state functional connectivity between major intrinsic networks varies substantially across individuals. Most analyses treat this variation as nuisance—individual differences to be averaged away in group-level contrasts. But it is not obvious that this variation is unstructured. We asked whether coupling among the DMN, CEN, and SN clusters into discrete modes in a transdiagnostic sample, and whether the resulting structure relates to psychiatric diagnosis.

The NIMH Research Domain Criteria (RDoC) initiative has argued for dimensional, mechanism-based approaches to psychopathology for over a decade [Insel et al., 2010], but has offered a framework without specifying which dimensions organize the variance. Triple-network coupling intensity is a candidate axis: the DMN, CEN, and SN serve distinct functional roles (self-referential processing, goal-directed control, and attentional switching, respectively), and the strength of their interaction at rest varies substantially across individuals [Menon, 2011]. Recent work within diagnostic categories has demonstrated that triple-network connectivity profiles can define neurobiological subtypes—for example, Jiang et al. [2020] identified two first-episode schizophrenia subgroups with distinct DMN-CEN-SN connectivity patterns associated with different cognitive profiles. Whether analogous coupling modes exist transdiagnostically—and whether they organize independently of diagnosis—has not been directly tested.

We tested this on a transdiagnostic sample of 249 subjects spanning four diagnostic categories, all scanned on a single instrument and processed with confound regression. Our analysis was exploratory: we applied unsupervised mixture modeling to between-network coupling values and asked whether the resulting structure relates to psychiatric classification. We interpret the

results in light of a broader theoretical framework (the Topological-Recursive Identity Model, TRIM; Campos 2026), which independently predicted discrete coupling phenotypes, though the empirical findings reported here stand without commitment to that framework.

2 Methods

2.1 Dataset

Data were drawn from the UCLA Consortium for Neuropsychiatric Phenomics (CNP), publicly available as OpenNeuro dataset ds000030 [Poldrack et al., 2016]. fMRIPrep-preprocessed derivatives were used, providing BOLD data in MNI152NLin2009cAsym standard space and confound regressors for each subject. Of 272 participants, 261 had complete fMRIPrep derivatives. After motion-based quality control (exclusion of subjects with mean framewise displacement > 0.5 mm), 249 subjects remained (Table 1).

Table 1: Sample demographics after fMRIPrep processing and motion QC.

Diagnostic Group	N	Excluded (FD)
Healthy Control	118	4
Bipolar Disorder	48	1
Schizophrenia	45	5
ADHD	38	1
Total	**249**	**11**

All participants were scanned on the same 3T Siemens Trio at UCLA using an identical protocol. Single-scanner acquisition eliminates inter-site scanner variance.

2.2 Preprocessing and Confound Regression

BOLD time series were extracted from fMRIPrep-preprocessed volumes (MNI152NLin2009cAsym space) using NiftiLabelsMasker (nilearn; Abraham et al. 2014) with z-score standardization. Thirteen confound regressors were regressed from the BOLD signal prior to connectivity estimation: framewise displacement (FD), 6 rigid-body motion parameters (3 translation, 3 rotation), 5 anatomical CompCor components (aCompCor00–04), and white matter signal.

Motion quality control: subjects with mean FD > 0.5 mm were excluded ($N = 11$). For the retained sample ($N = 249$), mean FD was 0.18 ± 0.15 mm and the median percentage of volumes exceeding FD > 0.5 mm was 5.8%.

2.3 Parcellation

Cortical regions were defined using the Schaefer 100-region atlas [Schaefer et al., 2018] mapped to the Yeo 7-network parcellation [Yeo et al., 2011]. Network assignment:

- **DMN**: all Schaefer parcels labeled "Default" ($n = 24$)
- **CEN**: all parcels labeled "Cont" (frontoparietal control; $n = 13$)
- **SN**: all parcels labeled "SalVentAttn" (salience/ventral attention; $n = 12$)

2.4 Coupling Metrics and Statistical Analyses

Full Pearson correlation matrices (100 × 100) were computed from the denoised time series for each subject. Three between-network coupling metrics were derived: mean DMN-CEN, DMN-SN, and CEN-SN correlation. Within-network coherence (within-DMN, within-CEN) was also computed.

Gaussian mixture models (1–5 components, BIC-selected) were fit in two configurations: (1) univariate, using DMN-CEN coupling alone; and (2) multivariate, using all three between-network metrics simultaneously (DMN-CEN, DMN-SN, CEN-SN). Bootstrap likelihood ratio tests ($k = 1$ vs. $k = 2$, 500 parametric iterations) assessed whether the 2-component model was significantly preferred. Hartigan's dip test [Hartigan & Hartigan, 1985], Shapiro-Wilk normality test, one-way ANOVA, pairwise t-tests, and χ^2 tests of independence (diagnosis × cluster) were computed.

3 Results

3.1 Univariate Analysis: DMN-CEN Coupling

BIC model comparison selected 2 components as optimal (ΔBIC = 29.3 over the single-component model). Bootstrap likelihood ratio test ($k = 1$ vs. $k = 2$, 500 iterations): $p < 0.001$. Shapiro-Wilk: $p < 0.001$ (skew = 1.12). Dip test: $p = 0.97$ (does not reject unimodality).

The 2-component GMM separates the sample into two clusters (Table 2).

Table 2: Cluster characteristics from 2-component univariate GMM (denoised).

Cluster	Mean DMN-CEN	N	%
Low-coupling	0.124	201	80.7
High-coupling	0.264	48	19.3

One-way ANOVA (DMN-CEN coupling ∼ diagnosis): $F = 1.129$, $p = 0.338$. No pairwise comparison between diagnostic groups reached significance (all $p > 0.16$).

3.2 Multivariate Analysis: Triple-Network Coupling

To test whether the clustering reflects coordinated structure across the triple-network system rather than variance in a single metric, a multivariate GMM was fit to all three between-network coupling values simultaneously (DMN-CEN, DMN-SN, CEN-SN).

BIC again selected 2 components (ΔBIC = 19.4). Bootstrap likelihood ratio test: $p < 0.001$ (observed LR = 74.6; null 95th percentile = 5.1). The two clusters are described in Table 3.

Table 3: Cluster characteristics from 2-component multivariate GMM (3D: DMN-CEN, DMN-SN, CEN-SN).

Cluster	DMN-CEN	DMN-SN	CEN-SN	N (%)
Low-coupling	0.121	0.029	0.108	189 (75.9%)
High-coupling	0.242	0.118	0.169	60 (24.1%)

Cluster assignments from the univariate and multivariate models agreed for 94.4% of subjects (adjusted Rand index = 0.76). The triple-network architecture clusters as a coordinated unit: all three between-network metrics are jointly elevated in the high-coupling cluster.

3.3 Diagnosis Does Not Predict Cluster Membership

χ^2 test of independence (diagnosis × multivariate cluster): $\chi^2 = 1.22$, $p = 0.748$, $df = 3$. Diagnostic category and cluster membership are statistically independent. The contingency table (Table 4) shows all four diagnostic groups distributed across both clusters in proportion to their base rates.

Table 4: Contingency table: diagnosis × multivariate cluster.

Diagnosis	Low-coupling	High-coupling
ADHD	27	11
Bipolar	36	12
Control	93	25
Schizophrenia	33	12

3.4 Three-Component Exploration

A 3-component multivariate model reveals monotonic scaling across all coupling metrics (Table 5).

Table 5: Coupling metrics across three multivariate GMM components. All three between-network metrics increase monotonically.

Component	N (%)	DMN-CEN	DMN-SN	CEN-SN
Comp. 1	138 (55.4%)	0.112	−0.003	0.072
Comp. 2	88 (35.3%)	0.181	0.101	0.166
Comp. 3	23 (9.2%)	0.308	0.199	0.261

The highest-coupling component accounts for 9.2% of the sample. BIC does not prefer the 3-component model over the 2-component model; determining whether finer structure exists requires a larger sample.

3.5 Sensitivity Analysis: Unprocessed Data

As a robustness check, the full analysis was repeated on unprocessed BOLD data (no fMRIPrep, no confound regression) from the same dataset ($N = 219$ after quality filtering). BIC again selected $k = 2$ (ΔBIC = 7.8, bootstrap LR $p < 0.001$). Two clusters emerged: low-coupling (76.3%, $\mu = 0.175$) and high-coupling (23.7%, $\mu = 0.344$). ANOVA across diagnostic groups: $F = 0.466$, $p = 0.706$. Confound regression shifts absolute coupling values downward, but the mixture structure and diagnosis independence are preserved across both pipelines.

3.6 Age Does Not Predict Coupling Architecture

Spearman correlation between DMN-CEN coupling and age: not significant (age range 21–50), suggesting a constitutional rather than developmental parameter.

4 Discussion

The main finding is that triple-network coupling shows mixture structure in this sample, and that the resulting clusters do not align with psychiatric diagnosis. The clustering survives confound regression (13 regressors including motion, aCompCor, and white matter signal), motion-based

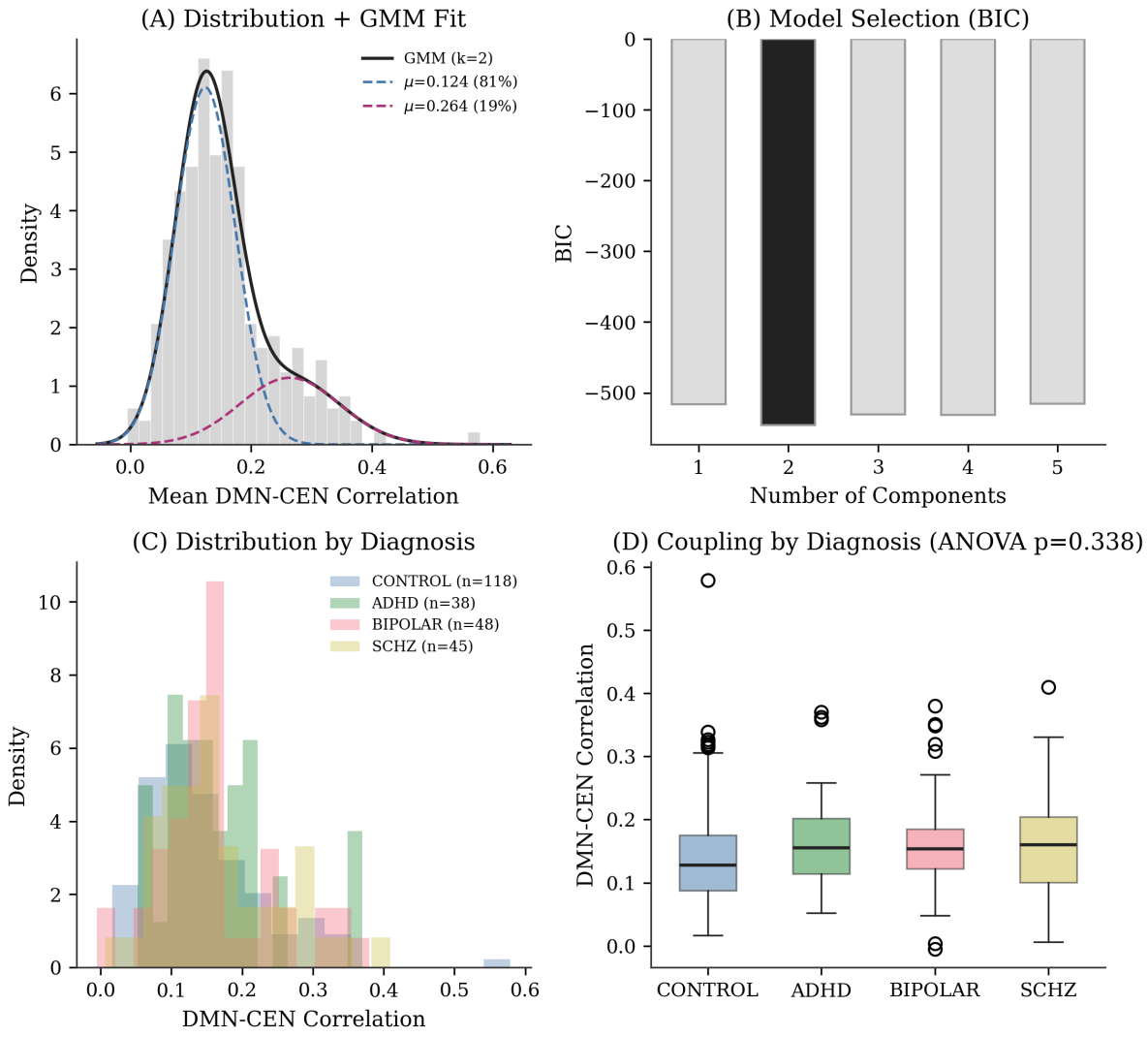

Figure 1: DMN-CEN coupling analysis ($N = 249$, denoised). (A) Distribution with 2-component GMM fit. (B) BIC model comparison ($k = 1$–5). (C) Per-diagnosis distributions. (D) Per-diagnosis boxplots (ANOVA $p = 0.338$).

exclusion, and extension from a single coupling metric to a multivariate triple-network analysis. Diagnostic category is statistically independent of cluster membership (χ^2 $p = 0.748$).

A person presenting with attentional difficulties, mood instability, or psychotic features could have either a low-coupling or high-coupling architecture. The diagnostic label does not distinguish between them.

Jiang et al. [2020] identified two first-episode schizophrenia subgroups with distinct triple-network connectivity profiles—one characterized by hypoconnectivity, the other by hyperconnectivity. Our results suggest that analogous coupling modes exist transdiagnostically: the same architectural axis is present across controls, ADHD, bipolar, and schizophrenia populations, and diagnostic category does not predict which mode a given individual occupies.

This aligns with longstanding critiques of categorical diagnosis. RDoC [Insel et al., 2010] has argued for dimensional approaches for over a decade but has not specified which dimensions organize the variance. Triple-network coupling topology is one candidate: it is measurable from standard resting-state fMRI, it clusters in this sample, and it does not track with diagnosis.

Whether stratifying by coupling architecture improves treatment outcomes is untested. These data show only that the axis exists and that it is diagnosis-independent.

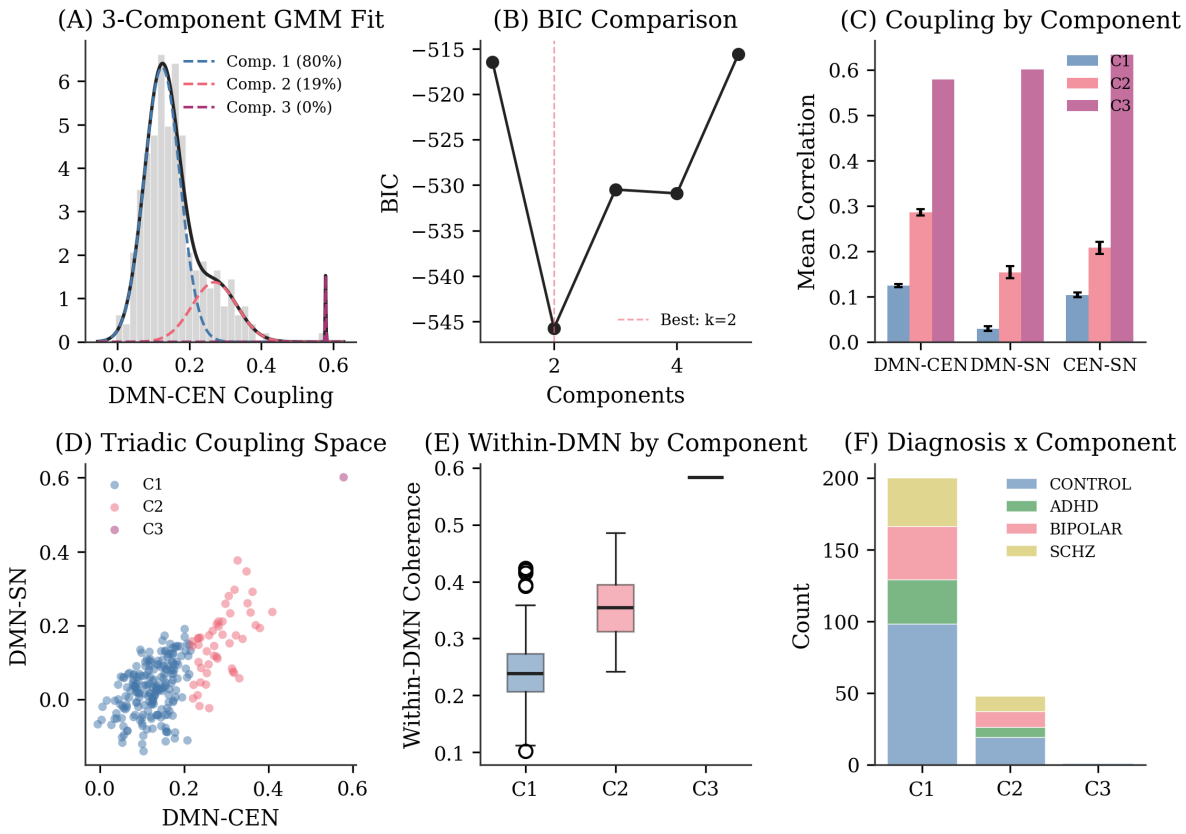

Figure 2: Three-component stress test. (A) 3-component GMM fit. (B) BIC comparison ($k = 1$–5). (C) Between-network coupling by component. (D) DMN-CEN vs. DMN-SN coupling space. (E) Within-DMN coherence by component. (F) Diagnosis × component distribution.

The TRIM framework [Campos, 2026], which motivated this analysis, labels the coupling components as Time-Division (low), Context-Dependent (moderate), and Phase-Lock (high), and predicts a population prevalence split of approximately 70–75% low-coupling vs. 25–30% high-coupling. The observed 75.9% / 24.1% split is consistent with this range. The 3-component model yields a highest-coupling group at 9.2%, within the predicted 5–10% prevalence. These correspondences are noted post hoc; the clustering and diagnosis independence do not depend on TRIM.

5 Limitations

What it shows:

- Triple-network coupling clusters into two modes in a transdiagnostic sample after confound regression.
- Diagnostic category does not predict cluster membership (χ^2 $p = 0.748$).
- The clustering is consistent across univariate and multivariate analyses (94.4% agreement).
- Coupling metrics scale monotonically in a 3-component model.

What it does not show:

- Causal relationships (cross-sectional, correlational design).

- That clusters correspond to qualitatively different experiences (requires behavioral validation).
- That a 3-component model is superior to a 2-component model (BIC prefers $k = 2$).
- Replication in an independent sample.
- Formal bimodality by shape-based criteria (dip test $p = 0.97$).

Methodological caveats: Motion-based exclusion removed a higher proportion of schizophrenia subjects (10%) than controls (3%). Psychiatric populations typically show higher motion, so this is not surprising, but it could affect the null finding. However, the same null result (ANOVA $p = 0.706$) was observed in the unprocessed analysis where no motion exclusion was applied.

ICA-based denoising (ICA-FIX) was not applied; confound regression with 13 regressors was used instead. While this addresses the most common sources of structured noise [Power et al., 2012], ICA-FIX provides more comprehensive denoising and is the standard for HCP data [Smith et al., 2013]. Replication on ICA-FIX-denoised data would further strengthen these findings.

The model-based and shape-based bimodality tests diverge: BIC and bootstrap LR strongly prefer two components, while the dip test does not reject unimodality. This is common when Gaussian components overlap at moderate sample sizes and would likely resolve with $N > 500$.

GSR was not applied; absolute coupling values are not comparable to GSR-corrected studies. Single-scanner acquisition eliminates inter-site variance but limits generalizability until replicated at other sites.

6 Data Availability

Dataset: UCLA Consortium for Neuropsychiatric Phenomics, OpenNeuro ds000030. Open access, no application required.

Code: The full analysis pipeline will be made available in a public repository upon publication.

Extracted data: Coupling values for all subjects (denoised and unprocessed) are published as CSV alongside this manuscript.

The analysis requires Python 3 with nilearn, scikit-learn, scipy, diptest, and matplotlib.

References

Abraham, A., Pedregosa, F., Eickenberg, M., Gervais, P., Mueller, A., Kossaifi, J., Gramfort, A., Thirion, B., & Varoquaux, G. (2014). Machine learning for neuroimaging with scikit-learn. *Frontiers in Neuroinformatics*, 8, 14.

Campos, A. (2026). The Topological-Recursive Identity Model: A thermodynamic framework for cognitive architecture. *Manuscript in preparation.*

Hartigan, J. A. & Hartigan, P. M. (1985). The dip test of unimodality. *The Annals of Statistics*, 13(1), 70–84.

Insel, T., Cuthbert, B., Garvey, M., Heinssen, R., Pine, D. S., Quinn, K., Sanislow, C., & Wang, P. (2010). Research Domain Criteria (RDoC): Toward a new classification framework for research on mental disorders. *American Journal of Psychiatry*, 167(7), 748–751.

Jiang, L., Zuo, C., Ye, D., Zhou, C., Zheng, J., Luk, K. N., Tang, J., Li, P., & Zang, Y. (2020). Aberrant triple-network connectivity patterns discriminate biotypes of first-episode medication-naive schizophrenia in two large independent cohorts. *Neuropsychopharmacology*, 45, 2217–2225.

Table 6: Summary statistics (denoised pipeline).

Parameter	Value
Dataset	UCLA CNP ds000030
Preprocessing	fMRIPrep + 13-regressor confound regression
N	249 (11 excluded, mean FD > 0.5 mm)
Parcellation	Schaefer 100 / Yeo 7
Univariate (DMN-CEN)	
GMM best k	2 (ΔBIC = 29.3)
Bootstrap LR	$p < 0.001$
ANOVA (Dx)	$F = 1.129$, $p = 0.338$ (n.s.)
Multivariate (DMN-CEN, DMN-SN, CEN-SN)	
GMM best k	2 (ΔBIC = 19.4)
Bootstrap LR	$p < 0.001$ (LR = 74.6)
χ^2 (Dx $\times$ cluster)	$\chi^2 = 1.22$, $p = 0.748$ (n.s.)
Univariate–multivariate agreement	94.4% (ARI = 0.76)
Dip test	$p = 0.97$ (does not reject unimodality)
Shapiro-Wilk	$p < 0.001$ (skew = 1.12)

Kass, R. E. & Raftery, A. E. (1995). Bayes factors. *Journal of the American Statistical Association*, 90(430), 773–795.

Menon, V. (2011). Large-scale brain networks and psychopathology: A unifying triple network model. *Trends in Cognitive Sciences*, 15(10), 483–506.

Power, J. D., Barnes, K. A., Snyder, A. Z., Schlaggar, B. L., & Petersen, S. E. (2012). Spurious but systematic correlations in functional connectivity MRI networks arise from subject motion. *NeuroImage*, 59(3), 2142–2154.

Poldrack, R. A., Congdon, E., Triplett, W., Gorgolewski, K. J., Karlsgodt, K. H., Mumford, J. A., Sabb, F. W., Freimer, N. B., London, E. D., Cannon, T. D., & Bilder, R. M. (2016). A phenome-wide examination of neural and cognitive function. *Scientific Data*, 3, 160110.

Schaefer, A., Kong, R., Gordon, E. M., Laumann, T. O., Zuo, X.-N., Holmes, A. J., Eickhoff, S. B., & Yeo, B. T. T. (2018). Local-global parcellation of the human cerebral cortex from intrinsic functional connectivity MRI. *Cerebral Cortex*, 28(9), 3095–3114.

Smith, S. M., Beckmann, C. F., Andersson, J., Auerbach, E. J., Bijsterbosch, J., Douaud, G., Duff, E., Feinberg, D. A., Griffanti, L., Harms, M. P., Kelly, M., Laumann, T., Miller, K. L., Moeller, S., Petersen, S., Power, J., Salimi-Khorshidi, G., Snyder, A. Z., Vu, A. T., Woolrich, M. W., Xu, J., Yacoub, E., Uğurbil, K., Van Essen, D. C., & Glasser, M. F. (2013). Resting-state fMRI in the Human Connectome Project. *NeuroImage*, 80, 144–168.

Yeo, B. T. T., Krienen, F. M., Sepulcre, J., Sabuncu, M. R., Lashkari, D., Hollinshead, M., Roffman, J. L., Smoller, J. W., Zöllei, L., Polimeni, J. R., Fischl, B., Liu, H., & Buckner, R. L. (2011). The organization of the human cerebral cortex estimated by intrinsic functional connectivity. *Journal of Neurophysiology*, 106(3), 1125–1165.